Supporting Information

Retrieving the co-assembly pathway of composite cellulose nanocrystal photonic films from their angular optical response

Bruno Frka-Petesic, Joel A. Kelly, Gianni Jacucci, Giulia Guidetti, Gen Kamita, Nathan P. Crossette, Wadood Y. Hamad, Mark J. MacLachlan and Silvia Vignolini**

1) Supporting tables and figures

Table S1. Summary of the main information deduced from the goniometer analysis of the film (Table S2 for complementary information).

$m_{\mathrm{BTMSE}}:m_{\mathrm{CNC}}$	$\lambda = n\,p(0)$	$p(0)$	p_{ka}	α	$\Phi^{\mathrm{ka}}_{\mathrm{CNC}}$	$c^{\mathrm{ka}}_{\mathrm{CNC}}$	$p_{\mathrm{ka}}\Phi^{\mathrm{ka}}_{\mathrm{CNC}}$
[wt/wt]	[nm]	[nm]	[µm]	[Ø]	[vol%]	[wt%]	[nm]
0:100	429	276	2.40	0.115	11.5	17.2	276
49:51	576	374	2.23	0.168	11.6	17.4	258
60:40	673	438	2.12	0.207	12.3	18.3	260
71:29	813	531	1.84	0.288	13.6	20.1	251
76:24	925	605	1.70	0.355	14.3	21.1	243

Table S2. Additional information deduced from the goniometer analysis.

$m_{\mathrm{BTMSE}}:m_{\mathrm{CNC}}$	$\Phi^{\mathrm{ka}}_{\mathrm{CNC}}$	$c^{\mathrm{ka}}_{\mathrm{CNC}}$	$\Phi^{\mathrm{ka}}_{\mathrm{BTMSE*}}$	$\Phi^{\mathrm{ka}}_{\mathrm{OS**}}$	$\Phi^{\mathrm{ka}}_{\mathrm{MeOH**}}$	$\Phi^{\mathrm{ka}}_{\mathrm{water**}}$	$[\mathrm{BTMSE^*}]^{\mathrm{ka}}$	$[\mathrm{MeOH^{**}}]^{\mathrm{ka}}$	$[\mathrm{MeOH^{**}}]^{\mathrm{ka,solv}}$	$\varepsilon_r{}^{**,\mathrm{ka}}$	$\sqrt{\varepsilon_r{}^{**,\mathrm{ka}}}$
[wt/wt]	[wt%	[wt%	[vol%]	[vol%]	[vol%]	[vol%]	[M][a)]	[M][a)]	[M][a)]	[Ø]	[Ø]
0:100	11.5	17.2	0.0	0.0	0.0	88.5	0.00	0.0	0.0	78.4	8.9
49:51	11.6	17.4	16.7	5.2	16.0	67.2	0.66	4.0	4.8	69.6	8.3
60:40	12.3	18.3	27.1	8.4	26.1	53.2	1.07	6.4	8.1	63.4	8.0
71:29	13.6	20.1	48.8	15.2	47.0	24.2	1.93	11.6	16.3	48.3	6.9
76:24	14.3	21.1	68.1	21.2	65.6[b)]	-1.1[b)]	2.70	16.2	25.2[b)]	32.7	5.7

[a)] $\Phi^{\mathrm{ka}}_{\mathrm{BTMSE*}}$ refers to the volume fraction of BTMSE at the kinetic arrest if no condensation has occurred, while $\Phi^{\mathrm{ka}}_{\mathrm{OS**}}$ in case of full condensation. $\Phi^{\mathrm{ka}}_{\mathrm{MeOH**}}$ is then the maximum released methanol volume fraction in the sample if no evaporation has occurred at the kinetic arrest, and $\Phi^{\mathrm{ka,solv}}_{\mathrm{MeOH**}}$ in the solvent only, and $\varepsilon_r{}^{**,\mathrm{ka}}$ is the corresponding relative permittivity of the methanol/water solvent only. [b)] Physically impossible values, indicating that some of the methanol must have evaporated.

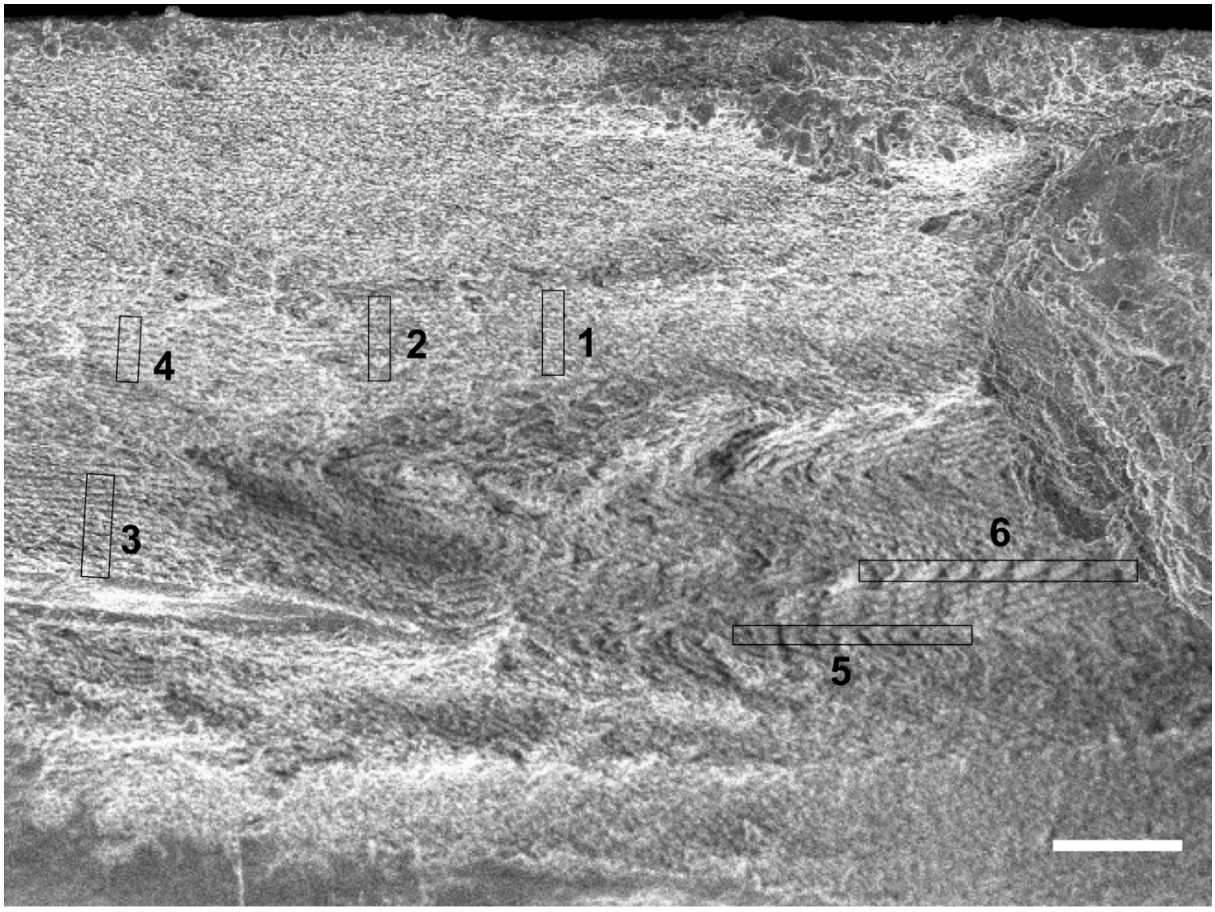

Figure S1. SEM image of the cross-section of a composite film (m_{BTMSE}: m_{CNC} = 60:40). The regions (1-6) were analyzed by profile plots (integrated over a width of 9 pixel) allowing for an estimation of the apparent pitch in the vertical and horizontal directions. This low magnification allows for seeing the surface of the film and compare with the domain tilt.

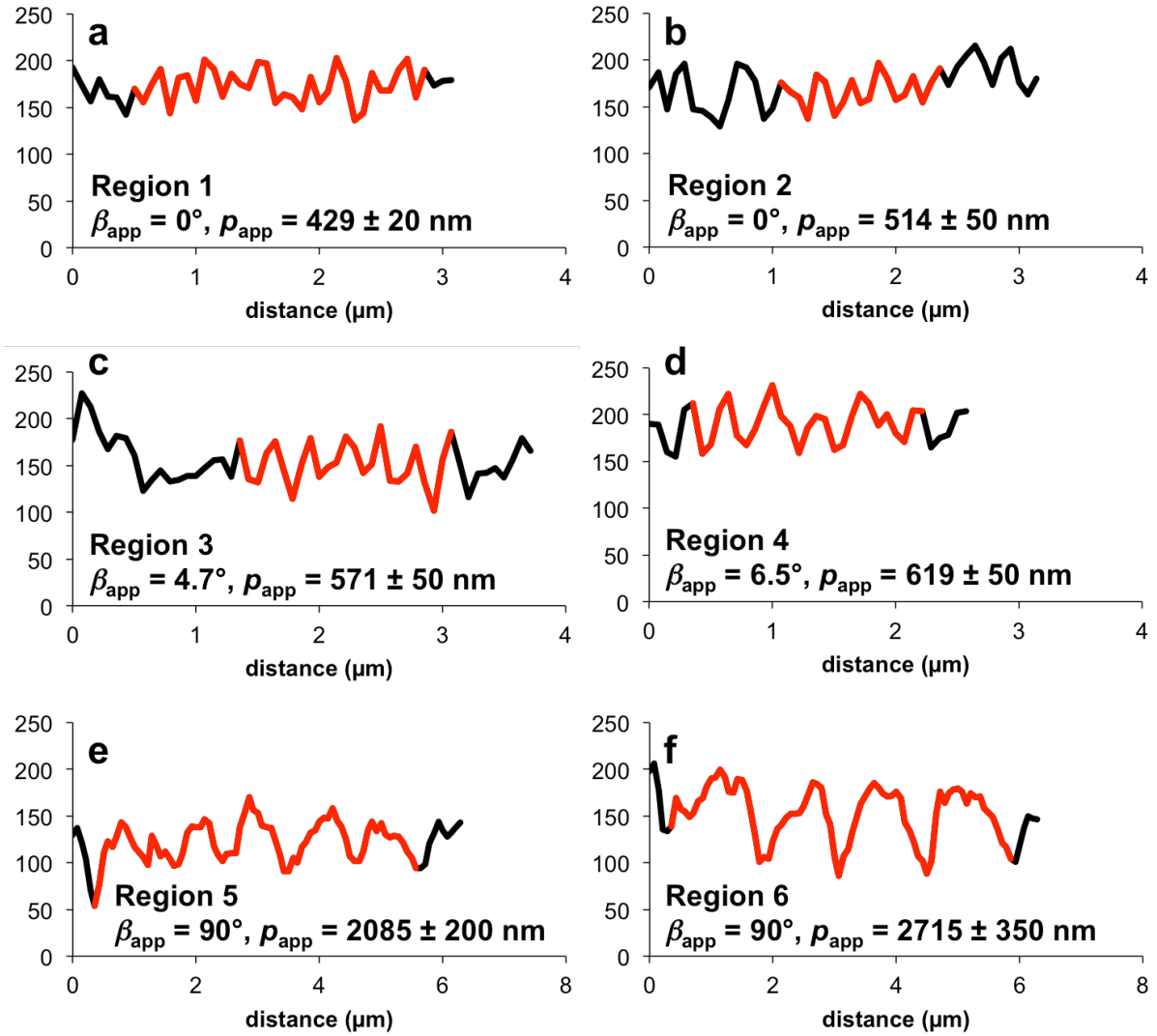

Figure S2. Gray scale intensity profile plots (in arbitrary unit), measured in the regions (1-6) of Figure S1 (sample m_{BTMSE}: m_{CNC} = 60:40), allowing for the determination of the apparent pitch p_{app} in the different directions, vertical and horizontal.

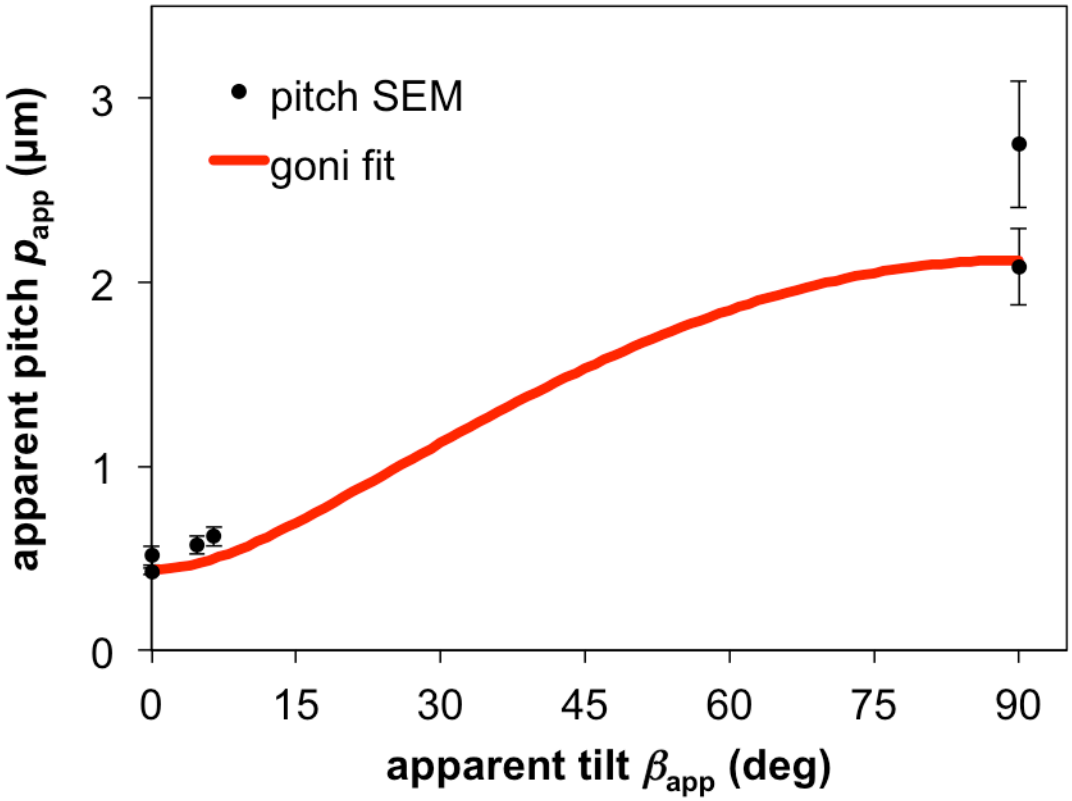

Figure S3. Reported apparent pitch values p_{app} measured in different directions of an SEM cross-section (sample m_{BTMSE}: m_{CNC} = 60:40), and compared with the angular pitch variation expected from our model and using α and p_{ka} obtained from the experimental goniometer data. The smallest apparent pitch p_{app} are consistent with the real pitch $p(\beta)$, while larger values are consistent with the artifact of domain misalignment.

2) Additional information on materials and methods

a) Sample preparation

Preparation of Cellulose Nanocrystals: CNC samples were provided by FPInnovations and were prepared using slightly different hydrolysis conditions from the cited reference.[1] For this specific batch, fully-bleached, commercial Kraft softwood pulp was first milled to pass through a 0.5 mm screen in a Wiley mill to ensure particle size uniformity and to increase surface area. Aliquots of concentrated sulphuric acid (95-98%) (Sigma-Aldrich) were diluted to 62 wt.% solutions. The milled pulp (60.0 g o.d.) was hydrolyzed in sulphuric acid (8.75mL of a sulphuric acid solution/g pulp) at a concentration of 62 wt.% and a temperature of 55 °C, respectively. The sulphuric acid solution was heated to the desired temperature (55 °C), added to the pulp in an Erlenmeyer flask in a hot water bath heated to the same temperature, and

allowed to hydrolyze the pulp under stirring with an impeller at high speed for 25 min. The cellulose suspension was then diluted with cold, deionized (DI) water (~10 times the volume of the acid solution used) to stop the hydrolysis, and allowed to settle overnight. The clear top layer was decanted off and the remaining white cloudy layer was centrifuged and washed twice with DI water. The suspension after the last centrifugation was then dialyzed against slow DI water using dialysis membrane tubes (12,000-14,000 molecular weight cut-off) until the water outside the dialysis membranes maintained at constant pH. After dialysis, the suspensions were diluted ~3 times with DI water owing to their high viscosity. Then, all suspensions were dispersed by subjecting them to ultrasound treatment using a VibraCell 750 Watts sonicator (Sonics & Materials, INC.) at 70% power for 30 minutes corresponding to an energy of ~ 9000 J/g. The sonicated suspensions were then filtered through a Whatman filter paper (#541 or #41) to remove any large particles. The purified suspensions were concentrated to the desired concentration using a rotavapor. The final CNC suspension was 3 wt.% and had a pH of 2.4.

Preparation of Organosilica/Cellulose nanocrystal (OS/CNC) Composite Films: Chiral nematic OS/CNC composite films were prepared by first sonicating the starting aqueous CNC suspension for 10 min. BTMSE was then added dropwise and the mixture was left to stir at room temperature for 1 h to obtain a homogeneous solution. The BTMSE/CNC mixtures were then cast into polystyrene Petri dishes (5 mL, Ø = 60 mm) and left to dry under ambient conditions (typically 18-24 h were required for complete drying). The different mass ratios of BTMSE:CNC used for the different chiral nematic composite samples are listed in Table 1. Chiral nematic CNC films were prepared using the same procedure but without the addition of BTMSE.

b) Sample characterization

Polarized optical microscopy (POM) was performed in reflection mode on a customized Zeiss Axio microscope using a halogen lamp (Zeiss HAL100) as a light source using Koehler illumination. Bright field (BF) images of the films were recorded with a 20× Epiplan Apochromat objective (NA = 0.6, WD = 1.7 mm) and a CCD camera (UI-3580LE-C-HQ, IDS). The reflected light was collected through a quarter-wave plate and a linear polarizing filter with adjustable mutual orientation to distinguish left- (LCP) and right-circularly polarized (RCP) light. The white balance reference was taken using a white Lambertian diffuser (USRS-99-010 AS-01158-060).

Spectroscopy: Reflection spectra were collected with a double-ended fiber (R200-7-SR, 00S-003413-01, Oceanoptics, placed in normal incidence with respect to the film surface) and analyzed with a spectrometer (AvaSpec-HS2048, Avantes), using a fiber-to-sample distance of 10 ± 0.5 mm and a white Lambertian diffuser as reference. White incident light was projected over a large surface (spot size Ø = 4.4 mm, area ~ 15 mm^2) in order to average out the variability of the local optical response.

Angular-resolved optical spectroscopy: Measurements were carried out using a lab-made goniometer: a xenon lamp (HPX-2000, Ocean Optics) was used as the light source and a spectrometer (AvaSpec-HS2048, Avantes) was used to analyze the scattered optical signal. The sample was mounted on a rotating stage in the center of the goniometer and illuminated with a collimated incident beam (light spot size Ø ~ 6 mm). A detector was mounted on an arm attached to a motorized rotation stage, and coupled the scattered light into an optic fiber connected to the spectrometer. The recorded light intensity was normalized with respect to a white Lambertian diffuser, while the exposure time was adjusted using an automatized high-dynamic-range (HDR) method.[2-4] Measurements were recorded at a fixed incident light angle θ_{in} = 30°, defined from the normal of the sample interface, and by scanning the scattered spectral intensity collected with the rotating detector.

Scanning Electron Microscopy (SEM) images were collected on a Leo Gemini 1530VP-Zeiss SEM. Samples were prepared by fracturing the films into small pieces and attaching them vertically to aluminum stubs so that the cross-section could be imaged. In order to prevent charging, the samples were attached using double-sided carbon adhesive tape and conductive silver paste, and coated with a thin layer of metal alloy using a sputter-coater (Emitech K550) with a Pd/Au target at a current of 55 mA for 6 s.

3) Comparison between pitch values from SEM and those predicted by the model.

The validity of our method and its accuracy can be assessed by comparing the estimated parameters with direct observations of film cross-sections in SEM. In **Figure 3b**, we report the pitch of the domains at zero tilt, $p(0) = \alpha\, p_{\mathrm{ka}}$, obtained either by goniometer analysis, by spectral analysis using the double-ended fiber in normal incidence, or by direct SEM observations of the film cross-sections, which are all in excellent agreement. The values we estimated for p_{ka} are expected to match with the pitch of domains tilted by 90°, which can also be compared to direct SEM observations. Indeed, cross-sections of polydomain films can occasionally capture the existence of these horizontal domains, and since vertical compression does not affect their horizontal periodicity, their pitch is expected to reflect the state of the suspension at the time of kinetic trapping, thus $p(90°) = p_{\mathrm{ka}}$ (**Figure S1**). As shown in **Figure 3c** for the sample where such a pattern is observed (m_{BTMSE}:m_{CNC} = 60:40), we have a good agreement with the value derived from goniometer analysis. This not only explains the apparent red-shift observed in off-specular conditions (**Figure 2c**), but also validates the robustness of our general approach.

4) Estimation of the OS and CNC volume fractions at the kinetic arrest.

a) Evaluation of mass and volume fractions in the final films

We control the mass of BTMSE and CNC combined and consider that in the final film all the BTMSE is fully condensed into OS. In order to evaluate the mass fraction c_{i} and volume

fraction Φ_i of CNC and OS in the final film, it is useful to consider a hypothetical intermediate (noted "itm") state where the film is completely dry but none of the BTMSE has yet initiated its condensation into OS. The mass fractions of BTMSE and CNC in that intermediate step are given by

$$c_{\mathrm{BTMSE}}^{\mathrm{itm}} = \mu/(1+\mu), \tag{S1}$$

$$c_{\mathrm{CNC}}^{\mathrm{itm}} = 1/(1+\mu), \tag{S2}$$

where $\mu = m_{\mathrm{BTMSE}}{:}\, m_{\mathrm{CNC}}$ is the mass ratio.

Their corresponding volume fractions are

$$\Phi_{\mathrm{BTMSE}}^{\mathrm{itm}} = \rho_{\mathrm{BTMSE}}^{-1} c_{\mathrm{BTMSE}}^{\mathrm{itm}} \Big/ \left(\rho_{\mathrm{CNC}}^{-1} c_{\mathrm{CNC}}^{\mathrm{itm}} + \rho_{\mathrm{BTMSE}}^{-1} c_{\mathrm{BTMSE}}^{\mathrm{itm}}\right), \tag{S3}$$

$$\Phi_{\mathrm{CNC}}^{\mathrm{itm}} = \rho_{\mathrm{CNC}}^{-1} c_{\mathrm{CNC}}^{\mathrm{itm}} \Big/ \left(\rho_{\mathrm{CNC}}^{-1} c_{\mathrm{CNC}}^{\mathrm{itm}} + \rho_{\mathrm{BTMSE}}^{-1} c_{\mathrm{BTMSE}}^{\mathrm{itm}}\right). \tag{S4}$$

In the final film, we assume then that all the BTMSE is condensed into OS. The mass fractions of CNC and OS in the final film can then be expressed as

$$c_{\mathrm{CNC}} = c_{\mathrm{CNC}}^{\mathrm{itm}} \Big/ \left(c_{\mathrm{CNC}}^{\mathrm{itm}} + c_{\mathrm{BTMSE}}^{\mathrm{itm}} M_{\mathrm{OS}}/M_{\mathrm{BTMSE}}\right), \tag{S5}$$

$$c_{\mathrm{OS}} = c_{\mathrm{BTMSE}}^{\mathrm{itm}} (M_{\mathrm{OS}}/M_{\mathrm{BTMSE}}) \Big/ \left(c_{\mathrm{CNC}}^{\mathrm{itm}} + c_{\mathrm{BTMSE}}^{\mathrm{itm}} M_{\mathrm{OS}}/M_{\mathrm{BTMSE}}\right). \tag{S6}$$

where M_{BTMSE} = 270.43 g mol^{-1} and M_{OS} = 132.22 g mol^{-1}.

The volume fractions in the film are then given by

$$\Phi_{\mathrm{CNC}} = \rho_{\mathrm{CNC}}^{-1} c_{\mathrm{CNC}} \Big/ \left(\rho_{\mathrm{CNC}}^{-1} c_{\mathrm{CNC}} + \rho_{\mathrm{OS}}^{-1} c_{\mathrm{OS}}\right), \tag{S7}$$

$$\Phi_{\mathrm{OS}} = \rho_{\mathrm{OS}}^{-1} c_{\mathrm{OS}} \Big/ \left(\rho_{\mathrm{CNC}}^{-1} c_{\mathrm{CNC}} + \rho_{\mathrm{OS}}^{-1} c_{\mathrm{OS}}\right), \tag{S8}$$

where we assumed the volumetric mass densities $\rho_{\mathrm{CNC}} = 1.600$ g cm^{-3}, $\rho_{\mathrm{BTMSE}} = 1.073$ g cm^{-3} and $\rho_{\mathrm{OS}} = 1.685$ g cm^{-3}, the latter being evaluated from the work of Wang et al. for non-porous OS.[6]

b) Volume fractions at the kinetic arrest

We introduce $\Phi_{\mathrm{CNC}}^{\mathrm{ka}}$ as the volume fraction of CNC at which the kinetic arrest occurs. From the onset of the kinetic arrest till the final formation of the film and the complete condensation

of BTMSE into OS, the volume of the sample decreases and thus the relative volume fraction of the CNCs increases from $\Phi_{\mathrm{CNC}}^{\mathrm{ka}}$ to Φ_{CNC}. If the volume loss is only due to a vertical compression, the ratio of the two volume fractions is given by

$$\Phi_{\mathrm{CNC}}^{\mathrm{ka}} = \alpha\, \Phi_{\mathrm{CNC}}, \tag{S9}$$

where α is the vertical scaling parameter that intervenes in our compression model.

This estimation is thus dependent on the hypothesis of pure vertical compression and to the accuracy of the determination of Φ_{CNC}, which relies on knowing the densities of the OS and CNC (both found in literature), their full condensation state (previous TGA measurements were consistent with that) and their respective mass fractions (known from masses of BTMSE and CNC used).

In order to estimate the concentration of OS species at the kinetic arrest, we first consider that no condensation has yet occurred at that point. The volume fraction of BTMSE (referred to as BTMSE* under such assumption) and water at the kinetic arrest can then be estimated as

$$\Phi_{\mathrm{BTMSE}^*}^{\mathrm{ka}} = \Phi_{\mathrm{CNC}}^{\mathrm{ka}} \left(\Phi_{\mathrm{BTMSE}}^{\mathrm{itm}}/\Phi_{\mathrm{CNC}}^{\mathrm{itm}}\right), \tag{S10}$$

$$\Phi_{\mathrm{water}^*}^{\mathrm{ka}} = 1 - \Phi_{\mathrm{BTMSE}^*}^{\mathrm{ka}} - \Phi_{\mathrm{CNC}}^{\mathrm{ka}}. \tag{S11}$$

The corresponding molar concentration of BTMSE is then given by

$$[\mathrm{BTMSE}^*]^{\mathrm{ka}} = \Phi_{\mathrm{BTMSE}^*}^{\mathrm{ka}}(\rho_{\mathrm{BTMSE}}/M_{\mathrm{BTMSE}}) \cdot 10^3 (\mathrm{cm}^3/\mathrm{L}). \tag{S12}$$

and its mass fraction as

$$c_{\mathrm{BTMSE}^*}^{\mathrm{ka}} = \rho_{\mathrm{BTMSE}}\, \Phi_{\mathrm{BTMSE}^*}^{\mathrm{ka}}/\rho_{\mathrm{ave}}^{\mathrm{ka}}, \tag{S13}$$

$$\rho_{\mathrm{ave}}^{\mathrm{ka}} = \rho_{\mathrm{BTMSE}}\, \Phi_{\mathrm{BTMSE}^*}^{\mathrm{ka}} + \rho_{\mathrm{CNC}}\, \Phi_{\mathrm{CNC}}^{\mathrm{ka}} + \rho_{\mathrm{water}}\, \Phi_{\mathrm{water}}^{\mathrm{ka}} \tag{S14}$$

where $\rho_{\mathrm{water}} = 1.000$ g cm^{-3}.

If instead we consider that all the BTMSE is condensed into OS when the kinetic arrest occurred, the volume fraction of OS at the kinetic arrest is then

$$\Phi_{\mathrm{OS}^{**}}^{\mathrm{ka}} = \Phi_{\mathrm{BTMSE}^*}^{\mathrm{ka}} \left(\frac{\rho_{\mathrm{BTMSE}}}{M_{\mathrm{BTMSE}}} \frac{M_{\mathrm{OS}}}{\rho_{\mathrm{OS}}}\right). \tag{S15}$$

As the full condensation of one BTMSE molecule releases six molecules of methanol, the suspension composition evolves from containing CNC, BTMSE and water to containing CNC, OS, water and methanol. However, both water and methanol evaporate and the exact ratio of methanol to water in the solvent at the point of kinetic arrest remains unknown. An upper limit for the concentration of methanol can still be estimated by assuming full condensation of OS and no evaporation of methanol at the moment of kinetic arrest:

$$[\mathrm{MeOH}^{**}]^{\mathrm{ka}} = 6[\mathrm{BTMSE}^{*}]^{\mathrm{ka}}, \tag{S16}$$

or in volume fraction in the sample, as

$$\Phi^{\mathrm{ka}}_{\mathrm{MeOH}^{**}} = [\mathrm{MeOH}^{**}]^{\mathrm{ka}}(M_{\mathrm{MeOH}}/\rho_{\mathrm{MeOH}}) \cdot 10^{-3}(\mathrm{L/cm^3}) , \tag{S17}$$

The volume fraction of water is then

$$\Phi^{\mathrm{ka}}_{\mathrm{water}^{**}} = 1 - \Phi^{\mathrm{ka}}_{\mathrm{CNC}} - \Phi^{\mathrm{ka}}_{\mathrm{OS}^{**}} - \Phi^{\mathrm{ka}}_{\mathrm{MeOH}^{**}}. \tag{S18}$$

Since the CNC and the OS do not contribute to the composition of the solvent, the volume fraction of methanol in the solvent is then given by:

$$\Phi^{\mathrm{ka,solv}}_{\mathrm{MeOH}^{**}} = \Phi^{\mathrm{ka}}_{\mathrm{MeOH}^{**}} / \left(\Phi^{\mathrm{ka}}_{\mathrm{MeOH}^{**}} + \Phi^{\mathrm{ka}}_{\mathrm{water}^{**}}\right). \tag{S19}$$

$$[\mathrm{MeOH}^{**}]^{\mathrm{ka,solv}} = [\mathrm{MeOH}^{**}]^{\mathrm{ka}} / \left(\Phi^{\mathrm{ka}}_{\mathrm{MeOH}^{**}} + \Phi^{\mathrm{ka}}_{\mathrm{water}^{**}}\right). \tag{S20}$$

The upper limit of this evaluation is the pure methanol, namely $\Phi^{\mathrm{ka,solv}}_{\mathrm{MeOH}^{**}} \leq 1$ and $[\mathrm{MeOH}^{**}]^{\mathrm{ka,solv}} \leq (\rho_{\mathrm{MeOH}}/M_{\mathrm{MeOH}}) \cdot 10^3(\mathrm{cm^3/L}) = 24.7$ M.

A value larger than this is unphysical and justifies applying an upper limit to $[\mathrm{MeOH}^{**}]^{\mathrm{ka,solv}} \leq 24.7$ M.

The solvent relative permittivity is then evaluated as

$$\varepsilon_{\mathrm{r}}^{**,\mathrm{ka}} = \Phi^{\mathrm{ka,solv}}_{\mathrm{MeOH}^{**}} \varepsilon_{\mathrm{r,MeOH}} + (1 - \Phi^{\mathrm{ka,solv}}_{\mathrm{MeOH}^{**}}) \varepsilon_{\mathrm{r,water}}. \tag{S21}$$

where $\varepsilon_{\mathrm{r,MeOH}} = 32.7$ and $\varepsilon_{\mathrm{r,water}} = 78.4$.

A visual illustration of the different calculations is provided in Figures S4-S8, for an increasing amount of BTMSE added. The bars are topped by the source of the information,

namely "goni" stands for goniometer (i.e., angular-resolved optical spectroscopy) and (S#) corresponds to the equations S# used, as provided in these Supporting Information.

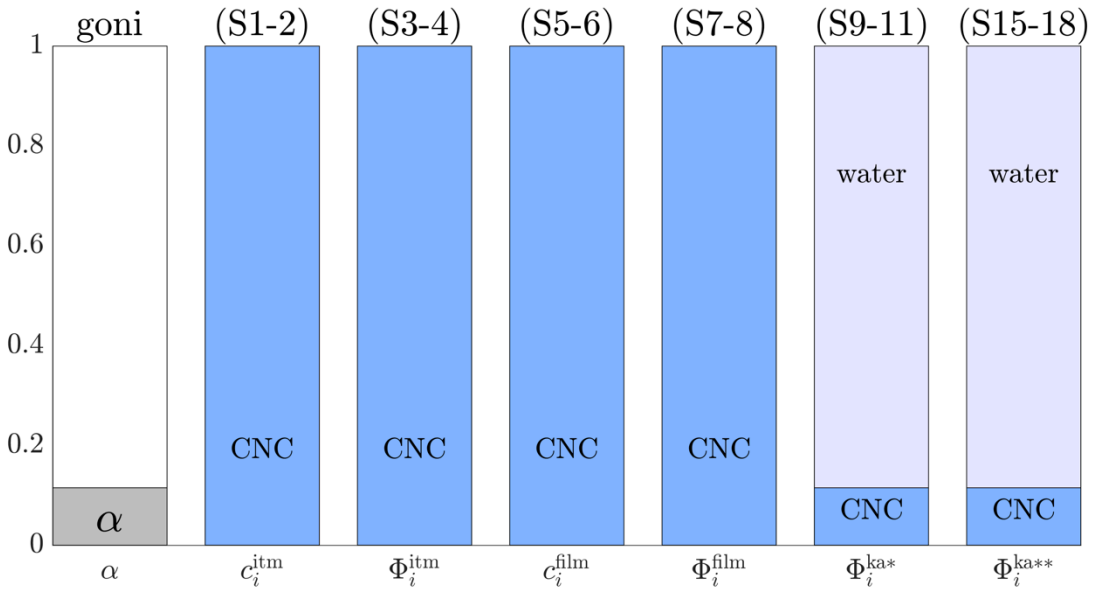

Figure S4. Visualization of the data processing for the sample m_{BTMSE}: m_{CNC} = 0:100.

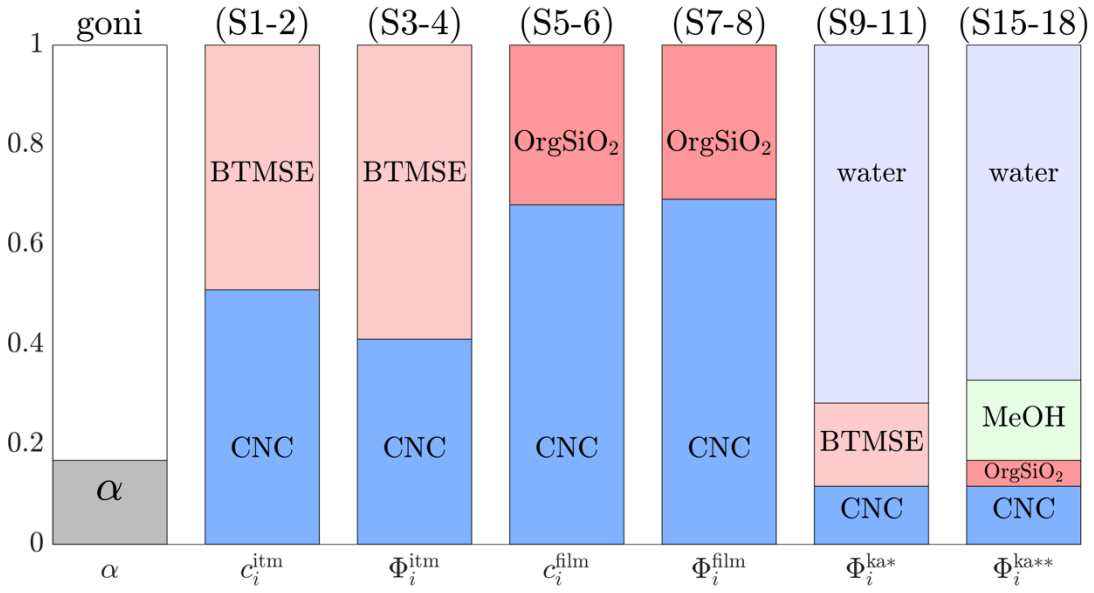

Figure S5. Visualization of the data processing for the sample m_{BTMSE}: m_{CNC} = 49:51.

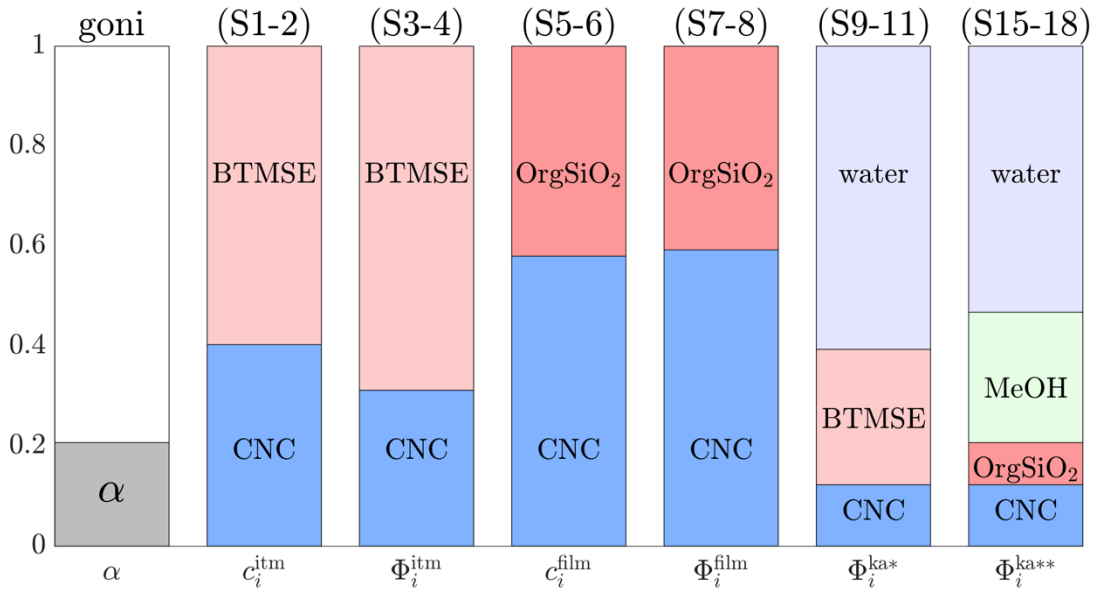

Figure S6. Visualization of the data processing for the sample m_{BTMSE}: m_{CNC} = 40:60.

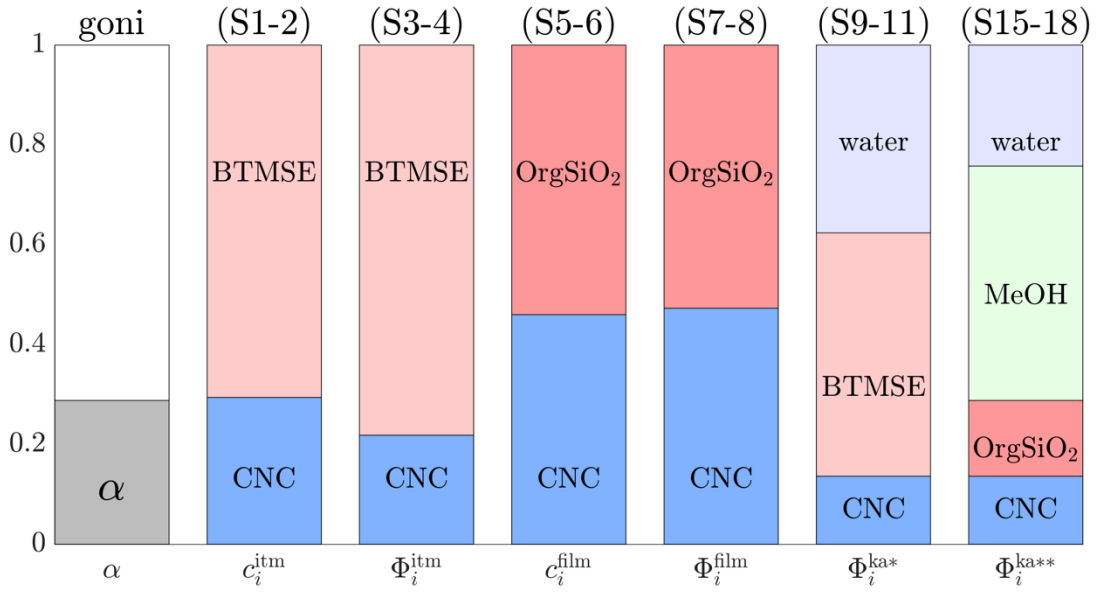

Figure S7. Visualization of the data processing for the sample m_{BTMSE}: m_{CNC} = 71:29.

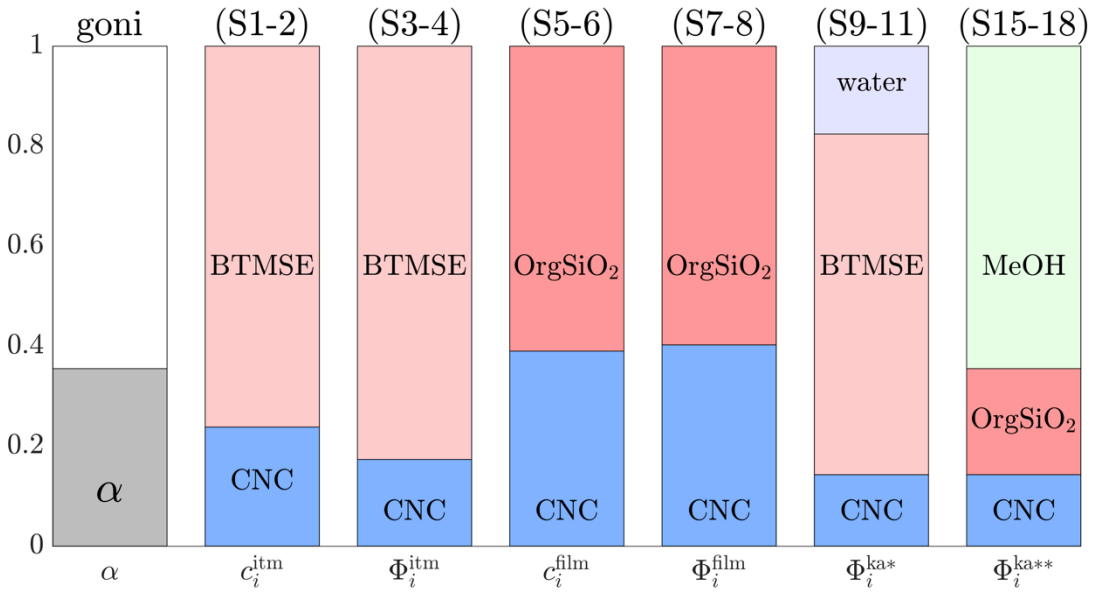

Figure S8. Visualization of the data processing for the sample m_{BTMSE}: m_{CNC} = 76:24.

c) Average optical index of OS/CNC films

The average optical index of the films were estimated as following:

$$n_{\mathrm{ave}}^{\mathrm{film}} = \sqrt{n_{\mathrm{CNC}}^2 \Phi_{\mathrm{CNC}} + n_{\mathrm{OS}}^2 \Phi_{\mathrm{OS}}} \quad \text{(S22)}$$

with n_{CNC} = 1.555 (from ref.[5]) and n_{OS} = 1.510.[6]

5) References

[1] W. Y. Hamad, T. Q. Hu, *Can. J. Chem. Eng.* **2010**, *88*, 392.

[2] B. Frka-Petesic, G. Guidetti, G. Kamita, S. Vignolini, *Adv. Mater.* **2017**, *29*, 1701469.

[3] G. Kamita, B. Frka-Petesic, A. Allard, M. Dargaud, K. King, A. G. A. G. Dumanli, S. Vignolini, *Adv. Opt. Mater.* **2016**, *4*, 1950.

[4] D.-P. Song, G. Jacucci, F. Dundar, A. Naik, H.-F. Fei, S. Vignolini, J. J. Watkins, *Macromolecules* **2018**, *51*, 2395.

[5] A. G. Dumanli, H. M. van der Kooij, G. Kamita, E. Reisner, J. J. Baumberg, U. Steiner, S. Vignolini, *ACS Appl. Mater. Interfaces* **2014**, *6*, 12302.

[6] W. Wang, D. Grozea, S. Kohli, D. D. Perovic, G. A. Ozin, *ACS Nano* **2011**, *5*, 1267.